PHYSICAL REVIEW B **76**, 174410 (2007)

Ultrafast vortex-core reversal dynamics in ferromagnetic nanodots

Ki-Suk Lee, Konstantin Y. Guslienko, Jun-Young Lee, and Sang-Koog Kim*
Research Center for Spin Dynamics and Spin-Wave Devices, Seoul National University, Seoul 151-744, Republic of Korea and Nanospintronics Laboratory, Department of Materials Science and Engineering, College of Engineering, Seoul National University, Seoul 151-744, Republic of Korea

(Received 31 August 2007; published 5 November 2007; corrected 13 November 2007)

To verify the exact underlying mechanism of ultrafast vortex-core reversal as well as the vortex state stability, we conducted numerical calculations of the dynamic evolution of magnetic vortices in Permalloy cylindrical nanodots under an oscillating in-plane magnetic field over a wide range of the field frequency and amplitude. The calculated results reveal different kinds of the nontrivial dynamic responses of vortices to the driving external field, including the vortex-core reversal. In particular, the results offer insight into the 10 ps scale underlying physics of the ultrafast vortex-core reversal driven by small-amplitude (~10 Oe) oscillating in-plane fields. This work also provides fundamentals of how to effectively manipulate the vortex dynamics as well as the dynamical switching of the vortex-core orientation.

DOI: 10.1103/PhysRevB.76.174410 PACS number(s): 75.40.Gb, 75.40.Mg, 75.60.Jk, 75.75.+a

The question of how fast magnetization (**M**) reversal occurs in bulk or finite-size magnets is one of longstanding, central issues in the research field of magnetism.[1,2] In particular, the **M** dynamics of a magnetic vortex (MV) in patterned magnetic elements of submicron or less size is of growing interest because of its nontrivial static and dynamic properties[3–15] as well as promising applications to ultrafast, high-density information-storage technology.[1,16] Over the past decade, the static microstructure of the MV ground state in submicron-size magnetic particles of little or zero anisotropy has been studied experimentally and theoretically,[4–6] and thus is now well known.[17] The MV can be used as an information carrier, because it has two discrete states of the vortex-core (VC) orientation (up and down) and two directions of in-plane **M** rotation. From an application point of view, the switching of the VC orientation by small magnetic fields is of great importance as the potential to be used in magnetic data storage, data processing, strong spin-wave generation, and others.[1,16] However, such switching is known to be possible only with the application of a strong static magnetic field stronger than 2.5 kOe along the VC orientation.[18] This VC switching also assumes the formation and movement of a magnetic singularity (Bloch point) along the dot thickness.[19] This process demands the overcoming of a huge energy barrier, and thus is not realistic, especially at low temperatures.

Very recently, the VC switching in Permalloy (Py) square dots was experimentally observed by applying a small-amplitude field pulse using time-resolved scanning transmission x-ray microscopy as well as by monitoring a change of the rotation sense of the VC gyrotropic motion during the reversal event.[20] It has been shown in Ref. 20 by micromagnetic simulations that the VC reversal can occur via a sequence of vortex-antivortex (V-AV) pair creation and annihilation processes. However, it is still unclear what is the true mechanism of such VC reversal because of insufficient time and spatial resolutions of modern experimental techniques. There is considerable discrepancy between simulated switching field magnitude (35 Oe) and experimentally observed magnitude (15 Oe) in Ref. 20. Hertel and Schneider[21] simulated the dynamic evolution toward the equilibrium of an artificial initial V-AV-V state in a Py platelet and provided a more detailed explanation of the VC dynamics. However, the case of opposite vortex polarizations practically important for the VC dynamic reversal and dynamical evolution of the initial single V state under the influence of a driving field was not considered in Ref. 21. In fact, the annihilation process of the V-AV pair was already observed numerically in Refs. 22 and 23. Through this process, considerable energy excess can be dissipated from the V-AV annihilation area in the form of spin waves. Following the ideas described in Refs. 22 and 23, strong spin-wave radiation using the VC polarization reversal was suggested.[24] A numerical study similar to Ref. 24 was also carried out very recently by Xiao *et al.*[25] However, the authors of Ref. 25 simulated the VC reversal leaving the open questions about the reversal mechanism, VC trajectories, and dependence of the reversal on the driving field parameters.

Despite the above recent studies on how the VC reversal occurs, its physical origin, the reversal criteria, and details of the VC trajectories during the reversal are still lacking. Thus, it is necessary to explore the dynamics of the MV reversal and corresponding reversal eigenmodes especially in magnetic nanodots more deeply and in more detail. Usually, **M** reversal is fast (~1 to 10 ns) in single-domain magnetic particles of <10 nm size and relatively slow in magnetically nonuniform particles of large size. In this Brief Report, we demonstrate an important exception to this rule by calculating ultrafast **M** reversal of a nonuniform MV state in relatively large magnetic particles (of ~100 nm lateral size). We report a universal phase diagram of MV dynamic responses to the driving in-plane oscillating field over a wide range of the field frequency and amplitude including conditions of the VC reversal and the VC trajectories.

To understand the exact physical mechanism of the VC reversal under an external driving field and to find a means to control it, we conducted numerical micromagnetic calculations of the MV dynamic properties in a Py cylindrical nanodot. In the micromagnetic modeling, we used a diameter of $2R=300$ nm and a thickness of $L=10$ nm for the Py dot. This model yields an initial **M** state of a single MV with its downward-core orientation (polarization $p=-1$) and counterclockwise in-plane **M** rotation as shown in the top of Fig. 1. The static vortex annihilation field[9] and the gyrotropic

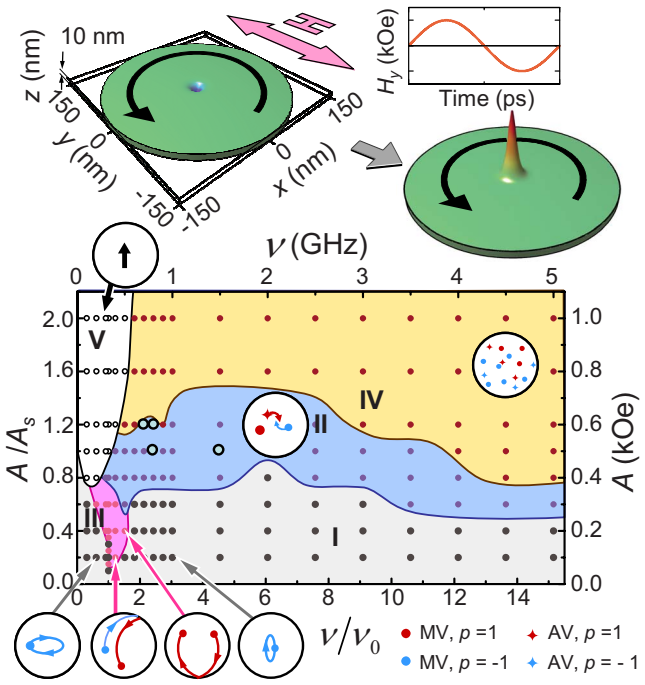

FIG. 1. (Color online) Phase diagram of the vortex dynamic response vs the frequency (ν) and amplitude (A) of a time-varying in-plane field in the Py cylindrical dot of R=150 nm and L =10 nm. The small solid spots of different colors indicate the data points in the A-ν plane, where the simulations were conducted. A_s and ν_0 denote the static vortex annihilation field and eigenfrequency of the MV gyrotropic motion in the given geometry, respectively. The boundaries are drawn according to the data points where the simulations were conducted. The round- and star-shaped spots in the dots indicate the MV and AV cores, respectively. Their blue (light gray) and red (dark gray) colors correspond to the downward (p=−1) and upward (p=+1) core orientations, respectively. The black arrow in region V represents an instantaneously saturated **M** state.

eigenfrequency[10] for the given model are A_s=500 Oe and ν_0=330 MHz, respectively. Over a wide range of the field amplitude A and frequency ν, covering A_s=500 Oe and ν_0 =330 MHz, we numerically calculated the dynamic response of the initial MV state under an oscillating in-plane magnetic field $\mathbf{H}(t)=A\sin(2\pi\nu t)\mathbf{y}$, based on the Landau-Lifshitz-Gilbert[26] (LLG) equation of **M** motion at T=0 K. Such form of the driving field allows us to explore vortex dynamical response in the resonance regime $\nu \approx \nu_0$ as well as far from the resonance, whereas in the case of the MV excitation by pulsed fields there is a mixture of different frequency harmonics.

Figure 1 shows the different dynamic regimes of the MVs in response to different A and ν values. The color-coded different regions, marked by I (gray), II (blue), III (pink), IV (yellow), and V (white), represent a low-amplitude gyrotropic motion, the periodic creation and annihilation process of a V-AV pair, a giant-amplitude gyrotropic motion (including the vortex escape from the dot and return to it), the nonperiodic process of the creation and annihilation of V-AV multipairs, and the instant dynamic saturation of **M** in the dot via the nucleation, movement, and annihilation of V-AV pairs, respectively. The representative trajectories of the individual VCs in the circular dot in the individual regions are schematically illustrated in the insets of Fig. 1 [see the supplementary information and supplementary Fig. 1 (Ref. 27) for the detailed description and VC trajectories]. Interestingly, the MV responds quite differently depending on A and ν, as shown in Fig. 1. The influence of the oscillating field on the MV is most effective when ν is close to ν_0. For low field frequencies ($\nu < \nu_0$) and low amplitudes, the gyrotropic motion is sufficient to respond to the oscillating magnetic field. For low ν and high A, the dynamic saturation state occurs (region V in Fig. 1). In this case, even though ν is low, the switching process between the two saturated states occurs over a short duration of a few nanoseconds, so any kind of process can be revealed in this regime. For high ν, the amplitude of the gyrotropic motion decreases with increasing ν. Therefore, the dominant process is the deformation of the total **M** structure of the vortex. This deformation increases with increasing A and ν, and their eigenfrequencies become higher (a few tens of gigahertz) than those of the gyrotropic motion. The VC gyrotropic motion leads to a deformation of the total dynamic **M** structure of MV due to the dynamic gyrotropic field, which is proportional to the moving vortex velocity.[13,28] We observe, with increasing A, a gradual transition from the simple gyrotropic motion of a single MV to the multi-V-AV behavior and, eventually, to a chaotic response, through the process of the creation and annihilation of the V-AV pairs as the result of an instability of the large dynamical deformation of the vortex structure. Consequently, over a wide range of A (above a certain threshold) and ν, the VC reversal occurs, in general, via the process of the creation and annihilation of a V-AV pair. Note that the elliptical VC trajectories observed in Ref. 20 in low field correspond to region I on the diagram in Fig. 1. The elliptical shape of the VC orbits arises due to differences between ν and ν_0.[29] The VC reversals observed by applying the field pulses in Refs. 20 and 25 are just particular cases of our phase diagram presented in Fig. 1, which correspond to area II.

Hereafter, we emphasize on the VC reversal mediated by the periodic creation and annihilation process of a V-AV pair, observed in a wide range of ν across ν_0 for sufficiently high A values. We consider only four different combinations of (ν,A) chosen due to their contrasting VC reversals, e.g., $(\nu/\nu_0, A/A_s)=(4.9,1)$, $(2.9,1)$, $(2.4,1.2)$, and $(2.1,1.2)$, as marked in region II (blue) of Fig. 1. First, for a case of $(\nu/\nu_0, A/A_s)=(4.9,1)$, the snapshot images of the vortex dynamical **M** distributions and the time evolution of the different energy contributions to the total dot energy are shown in Figs. 2(a) and 2(b), respectively. The representative trajectories of the VC motions in the circular dot for each case of (ν,A) are illustrated in Fig. 3.

Figures 2(a) and 2(b) show the exact mechanism of the VC switching in relation to the dot energy and **M** distribution evolution. The V-AV pair, having parallel core orientations opposite to that of the original VC orientation, nucleates, then the original vortex ($V^{\downarrow}$) annihilates with a new AV ($\bar{V}^{\uparrow}$), and the remaining final state is the MV with the switched VC polarization ($V^{\uparrow}$). From the snapshot images of the dynamic **M** distributions [Fig. 2(a)], we can clearly see

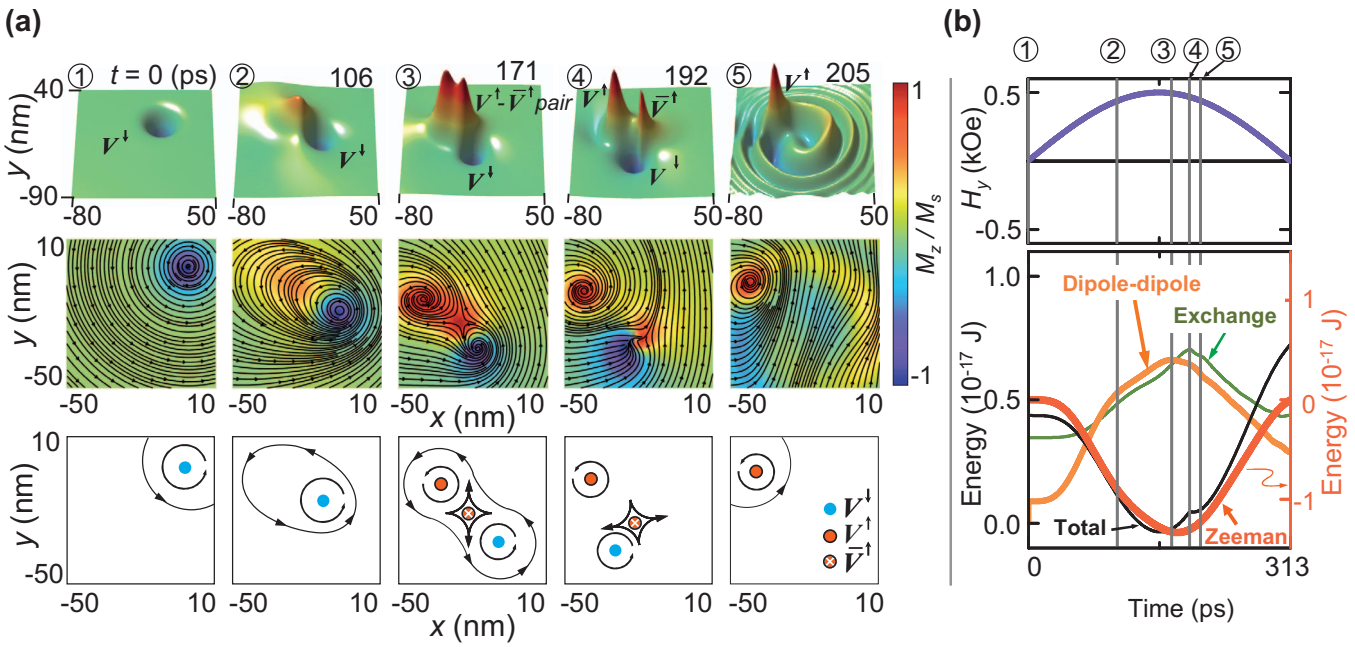

FIG. 2. (Color) (a) Underlying mechanism of the VC orientation switching mediated by the creation and annihilation of a V-AV pair and associated energy variation. The first and second rows display snapshot images of the local **M** distributions taken at the indicated times from the perspective and plane views, respectively, and the third row shows their schematic illustrations. The color and height of the surfaces in the first row indicate the local out-of-plane **M** normalized by the saturation value M_z/M_s. In the second row, the streamlines with the small arrows indicate the in-plane direction of **M**. The symbols $V^{\uparrow,\downarrow}$ and $\bar{V}^{\uparrow,\downarrow}$ represent MV and AV, respectively. Their superscripts indicate the "up" (↑) and "down" (↓) core orientations. (b) Temporal variation of the exchange, dipolar, and Zeeman energies and their sum for the core reversal of an original MV in the circular dot at $\nu/\nu_0=4.9$ and $A/A_s=1.0$.

each stage of the reversal process. With increasing field, the VC velocity increases, the entire vortex structure starts to deform, the in-plane curling **M** becomes elongated, and the out-of-plane **M** distribution of the VC becomes distorted. At $t=171$ ps, the VC deformation is maximized and then the V-AV ($V^{\uparrow}$-$\bar{V}^{\uparrow}$) pair nucleates. Such a trivortex state, $V^{\downarrow}$-$\bar{V}^{\uparrow}$-$V^{\uparrow}$, has indeed been observed in elliptic dots in a quasistatic regime.[30] The dipolar and exchange energies (they are approximately equal during the V-AV nucleation process) reach their maximum values at the indicated times, (3) and (4), respectively. After the moment, the nucleated AV and the original vortex move closer due to their attractive interaction[22,23] and then finally annihilate. Immediately after the V-AV annihilation, strong radial spin waves are emitted from the V-AV annihilation point [see snapshot (5) in the first row of Fig. 2(a)].[22,24] Meanwhile, the newly created vortex moves away from the annihilation point. The VC reversal is an ultrafast process (subnanosecond) and can be achieved in relatively low fields (~100 Oe) or extremely small fields (~10 Oe) for the case of $\nu\sim\nu_0$. This reversal phenomenon can be understood in relation to the energy variations with field or time. In order to respond to the Zeeman torque and to decrease the Zeeman energy, the original MV structure oscillates and deforms due to the gyrotropic field. This deformation of the **M** distribution increases with increasing **H**, leading to the concentration of the dipolar and exchange energies, and hence their energy densities markedly increase in the local area near the core region [see the supplementary Fig. 2 (Ref. 27)]. The out-of-plane **M** component in this area also increases as the in-plane **M** structure of the MV becomes more deformed. To decrease the dipolar energy, a V-AV pair eventually nucleates in this area; during the nucleation of the V-AV pair, the exchange energy increases while decreasing when the nucleated AV and the original MV structure annihilate. The deformation of the in-plane **M** structure of the MV decreases as the applied magnetic field decreases. These processes occur continuously and repeatedly in response to the oscillating field [supplementary movies 1(a), 1(b), and 1(c) illustrate this mechanism[27]].

In addition to the above-mentioned single event of the VC switching, we also report the finding that the VC orientation switches or does not switch during the VC reversal process depending on the field parameters. Figures 3(a)–3(d) show the individual VC reversals, with and without the VC switching oppositely to the original core orientation, for each time interval equal to a half period of the corresponding oscillating field. The process of the creation and annihilation of the V-AV pairs takes place one, two, three, and four times, respectively, as shown by the trajectories of the individual cores. The time evolutions of the VC trajectories for the cases of Figs. 3(a)–3(d) are shown in supplementary movies 2(a), 2(b), 2(c) and 2(d), respectively.[27] The MV with $p=+1$ starts its motion at point (1) at $H=0$ [Fig. 3(a)], and then it moves to point (2) at the moment (2). At the same moment (2), the V-AV pair with $p=-1$ nucleates at the marked site of the nucleation apart from the original MV. The newly formed AV moves to the original MV and annihilates with it, whereas the newly nucleated MV continues to move along the loop shape trajectory from point (3) to point (5). At moment (5), the V-AV pair again nucleates with $p=+1$. The new AV annihilates with the old MV, whereas the new MV

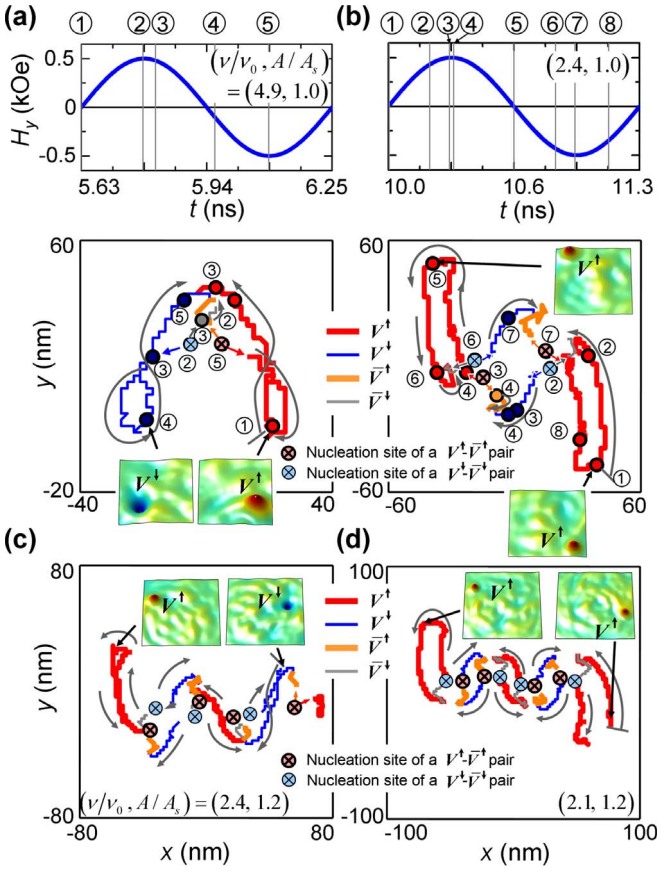

FIG. 3. (Color online) The trajectories of the individual VCs during one field period. The variation of the external field is shown in the upper row in (a) and (b). The thick red (dark gray), thin blue (dark gray), thick orange (light gray), and thin gray (light gray) colored lines indicate the trajectories of the cores of the MV with $p=+1$, the MV with $p=-1$, the AV with $p=+1$, and the AV with $p=-1$, respectively, as marked by the symbols. The number of the creation and annihilation events of the V-AV pairs is 1, 2, 3, and 4 in (a), (b), (c), and (d), respectively. The small gray colored arrows indicate the time flow and the direction of the motions of the individual vortices. In the bottom panels in (a) and (b), each open circle on the trajectories indicates the positions of each VC at the given moments, as noted by the numbers shown in the upper rows. The cross-mark-in-open-circle symbols denote the nucleation sites of the V-AV pairs at the indicated moments of (1) and (5) in (a) and (2), (3), (6) and (7) in (b). The time intervals for the MV (AV) core trajectories are $\Delta t=5.65-6.25$ ns, $\Delta t=10.00-11.25$ ns, $\Delta t=7.5-8.75$ ns, and $\Delta t=7.14-8.57$ ns in (a), (b), (c), and (d), respectively. In the insets, the snapshot images representing the corresponding core orientations at the marked times are shown for each case.

returns to point (1), and this process cycle repeats under the oscillating field. Note that each of the V-AV annihilation events leads to the emission of strong radial spin waves, that is, the MV adsorbs the energy of the external field and dissipates it via the spin waves. The radial spin waves propagate to the dot border and reflect from it, forming an interference pattern,[24] and then decrease their amplitude on the 100 ns time scale due to the damping in the equation of **M** motion. The spin-wave frequencies are of ~10 GHz and are determined mainly by the dot aspect ratio L/R.[14] In the case of Fig. 3(b), the two-time process of the creation and annihilation of V-AV pairs is more complex than that shown in Fig. 3(a), but the principal mechanism is the same, that is, the only difference is the two-time event of the nucleation and annihilation of the V-AV pairs.

Figure 3(c) shows that the VC reversal occurs three times for the half period and corresponds to the switch of the VC orientation, whereas Fig. 3(d) shows four times and no switch. If we consider that the external field has the form of a pulse field of the time duration of $1/(2\nu)$, the case of Fig. 3(a) or Fig. 3(c) corresponds to the VC switching to its opposite orientation but the case of Fig. 3(b) or Fig. 3(d) corresponds to no VC switching. The overall shape of the core trajectories is a zigzag curve. The number of the turning points in each case is determined by the number of the nucleation and annihilation events of the V-AV pairs during a half period of the field. The VCs are switched through only the odd-numbered events of V-AV pair creation and annihilation. Consequently, the VC switching can be effectively manipulated by tuning the amplitude and period of an oscillating in-plane magnetic field of weak amplitude (~10 Oe). We found that this unexpected dynamic process is typically mediated by the creation and annihilation of the V-AV pairs in the dot and is a pure dynamic process driven by the external oscillating field. This allows the **M** reversal to occur on the 10 ps time scale, making it faster than any **M** reversal previously known from either experiments or calculations. The calculated VC dynamical reversal can be observed in magnetic dots of any lateral shape.

In summary, we investigated dynamics of the vortex state in ferromagnetic nanodots in response to an in-plane ac magnetic field and identified the conditions for the ultrafast VC reversal and its underlying physics involving the creation-annihilation of the V-AV pairs and the escape of VC from the dot. The dynamic reversal mechanisms offer a principal opportunity to use the VCs for ultrafast information recording at frequencies in the subterahertz range as well as sources of the high-amplitude spin waves. The presented calculations open a route to controlled ultrafast switching of the VCs by a small-amplitude oscillating magnetic field. Any time-varying in-plane field, a field pulse, for instance, will create the similar MV dynamic response. The ultrafast VC switching is general for all dot shapes where the static MV is stable. The VC reversal can also be reached by applying sufficiently strong spin-polarized oscillating current with frequencies close to the vortex eigenfrequency.[31]

Note added in proof. Recently, we became aware of a paper by Hertel *et al.*,[32] which reports a similar vortex-core switching driven by a pulsed magnetic field. However, the phase diagram in Ref. 32 is very different from ours and the vortex- and/or antivortex-core trajectories in the course of the VC switching are not calculated.

This work was supported by Creative Research Initiatives (ReC-SDSW) of MOST/KOSEF.

*Corresponding author; sangkoog@snu.ac.kr

[1] S. D. Bader, Rev. Mod. Phys. **78**, 1 (2006).

[2] *Spin Dynamics in Confined Magnetic Structures II*, edited by B. Hillebrands and K. Ounadjela (Springer, Berlin, 2005).

[3] R. P. Cowburn, D. K. Koltsov, A. O. Adeyeye, M. E. Welland, and D. M. Tricker, Phys. Rev. Lett. **83**, 1042 (1999).

[4] T. Shinjo, T. Okuno, R. Hassdorf, K. Shigeto, and T. Ono, Science **289**, 930 (2000).

[5] A. Wachowiak, J. Wiebe, M. Bode, O. Pietzsch, M. Morgenstern, and R. Wiesendanger, Science **298**, 577 (2002).

[6] K. L. Metlov and K. Yu. Guslienko, J. Magn. Magn. Mater. **242-245**, 1015 (2002).

[7] S. B. Choe, Y. Acremann, A. Scholl, A. Bauer, A. Doran, J. Stohr, and H. A. Padmore, Science **304**, 420 (2004).

[8] K. S. Buchanan, P. E. Roy, M. Grimsditch, F. Y. Fradin, K. Yu. Guslienko, S. D. Bader, and V. Novosad, Nat. Phys. **1**, 172 (2005).

[9] K. Y. Guslienko, V. Novosad, Y. Otani, H. Shima, and K. Fukamichi, Phys. Rev. B **65**, 024414 (2002).

[10] K. Y. Guslienko, B. A. Ivanov, V. Novosad, Y. Otani, H. Shima, and K. Fukamichi, J. Appl. Phys. **91**, 8037 (2002).

[11] J. P. Park, P. Eames, D. M. Engebretson, J. Berezovsky, and P. A. Crowell, Phys. Rev. B **67**, 020403(R) (2003).

[12] K. Y. Guslienko, X. F. Han, D. J. Keavney, R. Divan, and S. D. Bader, Phys. Rev. Lett. **96**, 067205 (2006).

[13] V. Novosad, F. Y. Fradin, P. E. Roy, K. S. Buchanan, K. Y. Guslienko, and S. D. Bader, Phys. Rev. B **72**, 024455 (2005).

[14] K. Y. Guslienko, W. Scholtz, R. W. Cantrell, and V. Novosad, Phys. Rev. B **71**, 144407 (2005).

[15] A. Puzic, B. Van Waeyenberge, K. W. Chou, P. Fischer, H. Stoll, G. Schütz, T. Tyliszczak, K. Rott, H. Brückl, G. Reiss, I. Neudecker, T. Haug, M. Buess, and C. H. Back, J. Appl. Phys. **97**, 10E704 (2005).

[16] S. Choi, K.-S. Lee, and S.-K. Kim, Appl. Phys. Lett. **89**, 062501 (2006).

[17] The vortex structure has an in-plane curling **M** configuration and its core at the center. The core is a small area of 10–20 nm radius in which **M** deviates from the dot plane. The MV state is stable for sufficiently large lateral dot sizes (>20 nm) and thicknesses (>2 nm).

[18] N. Kikuchi, S. Okamoto, O. Kitakami, Y. Shimada, S. G. Kim, Y. Otani, and K. Fukamichi, J. Appl. Phys. **90**, 6548 (2001).

[19] A. Thiaville, J. M. Garcia, R. Dittrich, J. Miltat, and T. Schrefl, Phys. Rev. B **67**, 094410 (2003).

[20] B. Van Waeyenberge, A. Puzic, H. Stoll, K. W. Chou, T. Tyliszczak, R. Hertel, M. Fähnle, H. Brückl, K. Rott, G. Reiss, I. Neudecker, D. Weiss, C. H. Back, and G. Schütz, Nature (London) **444**, 461 (2006).

[21] R. Hertel and C. M. Schneider, Phys. Rev. Lett. **97**, 177202 (2006).

[22] K.-S. Lee, S. Choi, and S.-K. Kim, Appl. Phys. Lett. **87**, 192502 (2005).

[23] K. S. Lee, B. W. Kang, Y. S. Yu, and S. K. Kim, Appl. Phys. Lett. **85**, 1568 (2004).

[24] S. Choi, K.-S. Lee, K. Yu. Guslienko, and S.-K. Kim, Phys. Rev. Lett. **98**, 087205 (2007).

[25] Q. F. Xiao, J. Rudge, B. C. Choi, Y. K. Hong, and G. Donohoe, Appl. Phys. Lett. **89**, 262507 (2006).

[26] The LLG equation is given by $\partial \mathbf{M}/\partial t = -\gamma(\mathbf{M}\times\mathbf{H}_{eff}) + (\alpha/M_S)(\mathbf{M}\times\partial\mathbf{M}/\partial t)$, where α is the Gilbert damping constant, γ the gyromagnetic ratio, and $\mathbf{H}_{eff}$ the effective field containing individual contributions from the exchange, Zeeman, and dipolar interactions. We used the following material parameters for Py: the saturation magnetization $M_s = 8.6\times10^5$ A/m, the exchange stiffness constant $A = 1.3\times10^{11}$ J/m, the damping constant $\alpha = 0.01$, and the gyromagnetic ratio $\gamma = 2.21\times10^5$ m/A s. The unit cell size was $2\times2\times10$ nm^3. All simulations were done at $T = 0$.

[27] See EPAPS Document No. E-PRBMDO-76-082737 for two supplementary figures and seven movie files. For more information on EPAPS, see http://www.aip.org/pubservs/epaps.html

[28] A. Hubert and R. Schafer, *Magnetic Domains* (Springer, Berlin, 1998), Chap. 3.6.6.

[29] K.-S. Lee and S.-K. Kim, Appl. Phys. Lett. **91**, 132511 (2007).

[30] T. Okuno, K. Mibu, and T. Shinjo, J. Appl. Phys. **95**, 3612 (2004).

[31] S.-K. Kim, Y.-S. Choi, K.-S. Lee, K. Y. Guslienko, and D.-E. Jeong, Appl. Phys. Lett. **91**, 082506 (2007).

[32] R. Hertel, S. Gliga, M. Fähnle, and C. M. Schneider, Phys. Rev. Lett. **98**, 117201 (2007).